RSC Advances

ROYAL SOCIETY OF CHEMISTRY

www.rsc.org/advances

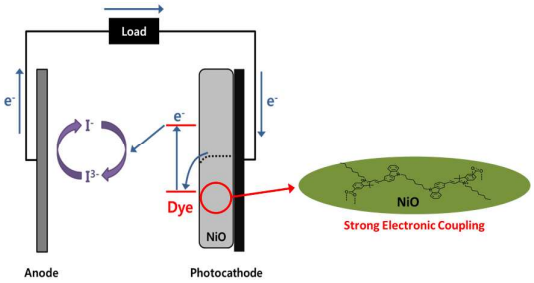

Carbazole dimer enhances the charge injection and reduces the charge recombination to exhibit superior p-type DSSCs performance.

RSC Advances

RSCPublishing

ARTICLE

Influence of the anchoring number in carbazole-based photosensitizer on the photovoltaic performance of p-type NiO dye sensitized solar cells†

Cite this: DOI: 10.1039/x0xx00000x

Received 00th January 2014,
Accepted 00th January 2014

DOI: 10.1039/x0xx00000x

www.rsc.org/

Ji Young Park[a], Bo Youn Jang[a], Chi Hwan Lee[a], Hyeong Jin Yun[a]*, Jae Hong Kim[a]*

The development of high performance p-type dye sensitized solar cells (DSSCs) is essential for producing tandem configurations that can overcome the theoretical limitations of single-junction DSSCs. This study evaluates a suitable organic dye for producing high performance p-type DSSCs. The photovoltaic properties of the carbazole monomer (MCBZ) and dimer (DCBZ) are examined to determine the effects of the molecular structure of the photosensitizer on the photovoltaic performance. MCBZ absorbs a larger amount of visible light photons with wavelengths between 400 and 600 nm, and provides better p-type DSSCs than conventional coumarin 343-sensitized solar cells. Furthermore, DCBZ exhibits better photovoltaic performance under standard global AM 1.5 solar conditions than the MCBZ-sensitized solar cells because of the synergistic effects of the enhanced electron injection efficiency and reduced charge recombination probability.

Introduction

Dye sensitized solar cells (DSSCs) have attracted considerable interest as the next-generation solar cells[1]. DSSCs are efficient photovoltaic devices, showing an overall peak power conversion of approximately 11 %. In addition, they have been the focus of economical solar electricity generation because the raw materials for producing DSSCs are relatively inexpensive and the manufacturing process is quite simple. Over the past two decades, a variety of dye-sensitized photoanodes have been developed for making highly efficient DSSCs. DSSCs with a wide-band gap p-type semiconductor (p-type DSSCs), such as NiO, have attracted increasing attention[2]. As shown in Scheme 1, p-type DSSCs work in an opposite manner to typical n-type DSSCs, in which the dye is photo-excited and transfers an electron to the electrolyte and a hole to the semiconductor (dye-sensitized hole injection). The combination of an n-type semiconductor-based photoanode with a p-type photocathode leads to a tandem configuration that can break through the theoretical limitations of single-junction DSSCs[3]. Moreover, these dye-sensitized photocathodes can also be applied to produce hydrogen under visible light irradiation[4].

The photo-sensitizing dye plays an important role in capturing photons, generating electron and hole pairs, and then transferring them to the electrolyte and semiconductor, respectively. A proper band structure is generally required to harvest solar light[2c-e]. Moreover, the molecular structure of organic photosensitizers should facilitate forward electron transfer from NiO to the photosensitizers with the suppression of backward electron transfer, which causes charge recombination[2e]. Thus far, coumarin 343 (C343, Fig. S1) has been used as the p-type photosensitizer. On the other hand, C343 shows a low extinction coefficient at the short wavelength visible light region

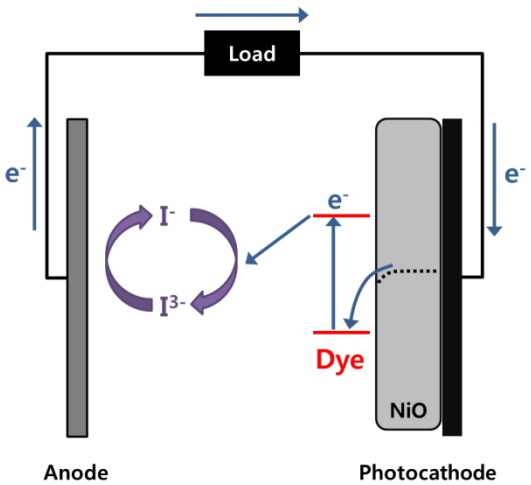

Scheme 1 Schematic diagram of charge transfer in a p-type DSSC.

around 400 nm, which limits the use of the solar spectrum[2c, 2d, 5]. C343 have shown a solar energy conversion efficiency of approximately 0.02 %[2c, 2d, 5]. Therefore, the development of novel p-type photosensitizers is essential for achieving high performance tandem-configured DSSCs. In this study, an efficient photosensitizing system capable of operating in the long wavelength range of the solar spectrum was fabricated by applying two types of carbazole-based chromophores dyes to p-type DSSCs. Carbazole-based chromophores dyes have been studied extensively in n-type DSSCs because of their

high molar extinction coefficient with visible light irradiation[6]. In addition, their synthetic process is convenient and their molecular design can be customized easily. Interestingly the highest occupied molecular orbital (HOMO) and the lowest unoccupied molecular orbital (LUMO) of carbazole-based chromophores dyes have a suitable band configuration with the band structure of NiO for applications to p-type DSSCs[6a]. Organic photosensitizers, such as mono (MCBZ) or double carbazole-based chromophores (DCBZ), were prepared and their photovoltaic properties for p-type DSSCs were compared. Indolium acceptor are used in these dyes, which has been recently utilized for enabling the dye to absorb the long wavelength visible light in p-type DSSCs[7]. The dyes have different numbers of anchoring moieties in their chromophores. Organic dyes containing double-electron acceptors/anchors were recently reported to be more efficient than the single-electron acceptor/anchor type because the former provides more electron extraction paths between the photosensitizing dye and TiO_2, forming stronger electronic coupling with TiO_2[8]. The effects of the molecular structure of the carbazole-based photosensitizer on the p-type DSSCs photovoltaic performance were investigated systemically. Their photovoltaic performance was examined by measuring the photocurrent density-voltage (J-V) characteristics under simulated solar light irradiation. The interfacial electron transfer processes were studied by measuring the incident photon to current efficiency (IPCE) and by electrochemical impedance spectroscopy (EIS).

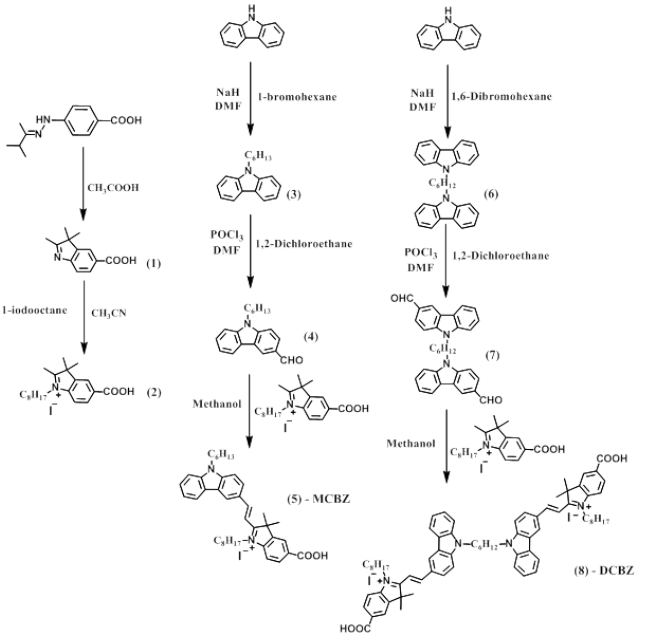

Scheme 2 Synthesis of MCBZ and DCBZ.

Experimental

Synthesis

Scheme 2 presents the scheme for the synthesis of MCBZ and DCBZ photosensitizer and their structures.

Trimethyl-3H-indole-5-carboxylic acid (1). 4-(2-(3-Methylbutan-2-ylidene)hydrazinyl)benzoic acid (11.5g, 52.2mmol) was dissolved in acetic acid (115 ml). The mixture was stirred for 24 hours under a nitrogen atmosphere. The solvent was then removed and the product was purified by column chromatography on silica gel with methanol : chloroform of 1:9 (v/v). The product was obtained as a yellow solid. Yield: 73%. ^{1}H NMR (300MHz, DMSO-d_6): δ 7.98 (s, 1H), 7.92 (d, J=8.1Hz, 1H), 7.51 (d, J=8.1Hz,1H), 2.25 (s, 3H), 1.27 (s, 6H).

5-carboxy-2,3,3-trimethyl-1-octyl-3H-indolium iodide (2). 2,3,3-Trimethyl-3H-indole-5-carboxylic acid (Product 1, 6.15g, 30.0mmol) and 1-iodooctane (21.85 ml, 120 mmol) were dissolved in 100 ml of acetonitrile, and stirred at 90 °C for 30 hours under a nitrogen atmosphere. The solvent was removed and the product was recrystallized with ethyl ether. The product was obtained as a yellow solid. Yield: 61 %. ^{1}H NMR (300MHz, DMSO-d_6) : δ 8.38 (s, 1H), 8.15 (d, J=8.3Hz, 1H), 8.07 (d, J=8.3Hz, 1H), 4.45 (t, J=7.5Hz, 2H), 2.87 (s, 3H), 1.57 (s, 6H), 1.45-1.10 (m, 12H), 0.83 (t, J=5.5Hz,3H).

9-hexyl-9H-carbazole (3). Carbazole (12g, 71.76 mmol), 1,6-dibromohexane (14.21 g, 86.08 mmol) and NaH (3.44 g, 143.35 mmol) were dissolved in 100 ml of dimethylformamide (DMF), and stirred at 60 °C for 4 hours. After the reaction, the product was separated by extraction using water and chloroform. The supernatant was then dried with $MgSO_4$. A white solid was obtained by removing the organic solvent followed by recrystallization with methanol. Yield: 89.44 %. 1H NMR (300 MHz, DMSO-d_6): δ 7.20 (d, J=5.7 Hz, 2H), 7.14 (d, J=6.9 Hz, 2H), 6.99 (d, J=8.1 Hz, 2H), 6.91 (t, J=7.2 Hz, 2H), 3.84 (t, J=6.9 Hz, 2H), 1.67-1.60 (m, 2H), 1.41-1.27 (m, 2H), 1.23-1.19 (m, 4H), 0.86-0.80 (m, 3H).

10-hexyl-10H-phenothiazine-3-carbaldehyde (4). 10-Hexyl-10H-phenothiazine (10 g, 35.3mmol) was then dissolved in 80 ml of 1,2-dichloroethane. Phosphorus oxychloride (27.06 g, 176.5 mmol) was added slowly to this mixture under reflux for 2 hours. Subsequently, the mixture was neutralized with Na_2CO_3. A yellow solid was obtained by recrystallization by removing the solvent. Yield: 94%. ^{1}H NMR (300MHz, DMSO-d_6): δ 9.83 (s, 1H), 7.77 (d, J=8.1Hz, 1H), 7.64 (s, 1H), 7.28-7.02 (m, 5H), 4.02-3.97 (m, 2H), 1.76-1.71 (m, 2H), 1.43 (s, 2H), 1.30 (s, 4H), 0.87 (s, 3H).

(E)-5-carboxy-2-(2-(9-hexyl-9H-carbazol-3-yl)vinyl)-3,3-dimethyl-1-octyl-3H-indolium (5) - (MCBZ). 10-hexyl-10H-phenothiazine-3-carbaldehyde (Product 4, 1g, 3.58 mmol) and 5-Carboxy-2,3,3-trimethyl-1-octyl-3H-indolium iodide (Product 2, 2.06g, 4.65 mmol) were dissolved in 35 ml of methanol. 5-carboxy-2,3,3-trimethyl-1-octyl-3H-indolium iodide (Product 2) (0.23 g, 0.514mmol) was added slowly to the mixture under reflux for 12 hours. A dark red product was obtained by recrystallization with ethyl acetate. Yield: 50 %. ^{1}H NMR (300 MHz, DMSO-d_6) : δ 9.11 (s, 1H) ,8.64 (d, J=16.2Hz, 1H), 8.41 (s, 2H), 8.19 (q, 2H), 7.66 (d, J=9Hz, 1H), 7.84 (d, J=8.4Hz, 1H), 7.20 (t, 2H), 7.61 (t, J=6.9Hz, 1H), 7.37 (t, J=6.9Hz, 1H), 4.70 (s, 2H), 4.50 (s, 2H), 1.88 (s, 10H), 1.26-1.19 (m, 16H), 0.79 (q, 6H). ^{13}C NMR (600MHz, DMSO-d_6): 182.859, 166.474, 157.492, 144.134, 143.942, 143.513, 140.816, 1303615, 130.469, 129.167, 127.044, 125.940, 125.710, 123.856, 123.097, 122.231, 120.713, 120.621, 114.567, 110.551, 108.551, 51.762, 45.999, 42.665, 31.039, 30.802, 28.449, 28.428, 28.395, 27.882, 26.035, 25.897, 25.690, 21.919, 21.904, 21.866, 13.819, 13.734, 13.696. Its mass spectrum is presented Fig. S2(A), and this has a good agreement of the molecular structure of MCBZ.

1,6-di(9H-carbazol-9-yl)hexane (6). Carbazole (11.99 g, 71.70mmol), 1,6-dibromohexane (7 g, 28.69 mmol) and NaH (3.44 g, 143.35 mmol) were dissolved in 100 ml of DMF, and stirred at 60 °C for 4 hours. After the reaction was complete, the product was separated by extraction using water and chloroform. The supernatant was dried with $MgSO_4$. A white solid was obtained by removing the organic solvent followed by recrystallization with methanol. Yield:

89.44 %. ^{1}H NMR (300MHz, $CDCl_3$): 8.11 (d, J=7.5Hz, 4H), 7.43 (d, J=7.4Hz, 4H), 7.34 (t, J=8.1Hz, 4H), 7.23 (t, J=7.8 Hz, 4H), 4.25 (t, J=6.9 Hz, 4H), 1.83–1.81 (m, 4H), 1.41–1.39 (m, 4H).

9,9'-(hexane-1,6-diyl)bis(9H-carbazole-3-carbaldehyde) (7). 1,6-di(9H-carbazol-9-yl)hexane (Product 6, 5g, 12.00mmol) and DMF (17.54 g, 240.06 mmol) were dissolved in 50 ml of dichloroethane. Phosphorus oxychloride (36.80 g, 240.06 mmol) was then added slowly to this mixture under reflux at 110 °C for 2 hours. After reaction, the product was separated by extraction using water and chloroform. The supernatant was purified by column chromatography on silica gel with chloroform : hexane at a V/V ratio of 1:3. A white solid was obtained. Yield: 67.5 %. ^{1}H NMR (300MHz, $CDCl_3$) : 10.04 (s, 2H), 8.73 (s, 2H), 8.27 (d, J=7.8Hz, 2H), 7.94 (d, J=8.4Hz, 2H), 7.70 (d, J=8.7Hz, 2H), 7.62 (d, J=8.1 Hz, 2H), 7.50 (t, J=7.2Hz, 2H), 7.29 (t, J=7.5Hz, 2H), 4.39 (t, J=6.9Hz, 4H), 1.71 (m, 4H), 1.30 (m, 4H).

2,2'-((1E,1'E)-(9,9'-(hexane-1,6-diyl)bis(9H-carbazole-9,3-diyl))bis(ethene-2,1-diyl))bis(5-carboxy-3,3-dimethyl-1-octyl-3H-indol-1-ium) iodide - (DCBZ). 9,9'-(hexane-1,6-diyl)bis(9H-carbazole-3-carbaldehyde) (Product 7, 0.7g, 1.48mmol) and 5-carboxy-2,3,3-trimethyl-1-octyl-3H-indolium iodide (Product 2, 2.06g, 3.70mmol) were dissolved in 35 ml of methanol. 5-Carboxy-2,3,3-trimethyl-1-octyl-3H-indolium iodide (Product 2) (0.23 g, 0.514mmol) was added slowly to this mixture under reflux for 12 hours. A black product was obtained by recrystallization with ethyl acetate. Yield: 80.24 %. ^{1}H NMR (300MHz, DMSO-d_6) : 9.11 (s, 2H), 8.80 (d, J=15.9, 2H), 8.42 (s, 2H), 8.39 (d, J=8.4, 2H), 8.23 (d, J=7.5, 2H), 8.18 (d, J=8.7, 2H), 7.98 (d, J=8.7, 2H), 7.82 (d, J=8.7, 2H), 7.72 (d, J=16.2, 2H), 7.68 (d J=4.8, 2H), 7.57 (t, J=7.5, 2H), 7.38 (t, J=7.2, 2H), 4.71 (t, 4H), 4.46 (t, 4H), 1.89 (s, 10H), 1.5-1.16 (m, 28H), 0.73 (t J=6, 6H). ^{13}C NMR (600MHz, DMSO-d_6): 183.152, 166.782, 157.746, 144.419, 144.181, 143.806, 141.070, 130.930, 130.777, 129.681, 127.313, 126.026, 124.156, 123.435, 122.546, 121.036, 120.983, 114.905, 110.790, 110.721, 108.882, 52.062, 46.345, 42.858, 31.316, 28.741, 28.710, 28.596, 28.404, 28.189, 26.350, 26.281, 25.967, 22.181, 14.004. Its mass spectrum is presented Fig. S2(B), and this has a good agreement of the molecular structure of DCBZ.

Characterization

All ^{1}H nuclear magnetic resonance (NMR) spectra were recorded on a Varian Mercury NMR 300 Hz spectrometer using $CDCl_3$ and DMSO-d_6 purchased from Cambridge Isotope Laboratories, Inc. ^{13}C NMR spectra were recorded on a Varian Mercury NMR 600MHz spectrometer using CDCl3 and DMSO-d_6. Elemental analysis was performed at the Center for Organic Reactions using an elemental analyzer (EA1112, Thermo Electron Corporation). The optical extinction spectra were recorded using a UV/vis/NIR spectrophotometer (845X, Agilent). Cross-section images of the NiO/FTO electrode were taken by scanning electron microscopy (SEM, S-4800, Hitachi, LTD). The microstructure of NiO was examined by X-ray diffraction (XRD, MPD for bulk (powder), PANalytical) using CuKα radiation (wavelength = 0.154 nm). The Fourier transform infrared (FT-IR, Perkin Elmer) spectra were obtained using a Miracle single bounce diamond ATR cell from PIKET Technologies. The redox properties of the dyes are examined by cyclic voltammetry (IVIUMSTAT, IVIUM).The electrolyte solution is 0.10 M tetrabutylammonium hexafluo-rophosphate ($TBAPF_6$) in freshly dried dimethylformamide (DMF). Ag/AgCl and Pt wire (0.5 mm in diameter) electrodes are used as the reference and counter electrodes, respectively. The scan rate is 30 mV/s. The measured potential is calibrated with respect to the redox potential of ferrocene.

2.3. Assembly and Characterization of the DSSCs.

A conducting glass substrate (FTO; TEC8, Pilkington, 8 Ω/cm^2, thickness of 2.3 mm) was cleaned in ethanol by ultrasonication. A NiO paste (NiO particles size: approximately 8.03nm) was prepared using ethyl cellulose (Aldrich) and terpineol (Aldrich) [9]. The prepared NiO paste was coated on a pre-cleaned glass substrate using the doctor-blade method, and sintered at 450 °C for 30 min. For dye adsorption, the annealed NiO electrodes were immersed in a solution of each dye (0.3 mM in ethanol). The Pt counter electrodes were prepared by the thermal reduction of a thin film formed from 7 mM H_2PtCl_6 in 2-propanol at 400 °C for 20 min. The dye-adsorbed NiO electrode and Pt counter electrode were assembled using a 60 μm-thick Surlyn (Dupont 1702) layer. A liquid electrolyte was introduced through a pre-punctured hole on the counter electrode. The electrolyte was composed of lithium iodide (LiI, 0.5 M) and iodine (I_2, 0.05 M) in propylene carbonate. The J-V characteristics of the prepared DSSCs were measured under 1 sunlight intensity (100 mW/cm^2, AM 1.5), which was verified using an AIST-calibrated Si-solar cell (PEC-L11, Peccell Technologies, Inc.). Three solar cells were fabricated under each condition. The J-V curves were obtained from the solar cell showing medium efficiency among the three tested-samples. The monochromatic IPCEs were plotted as a function of the wavelength using an IPCE measurement instrument (PEC-S20, Peccell Technologies Inc.). Electrochemical impedance spectroscopy (EIS) was performed using a computer-controlled potentiostat (IVIUMSTAT, IVIUM) over the frequency range, 10 kHz - 100 mHz, with an AC voltage amplitude of 10 mV at 0 V vs. the open circuit voltage (V_{OC}) in a two electrode measurement. The impedance spectra were interpreted using a nonlinear least-square fitting procedure on commercial software (ZView 2, Scribner Associates Inc.).

Results and discussion

Band structures

Fig. 1 shows the absorbance spectra of C343, MCBZ and DCBZ. The concentration of each dye in ethanol is 0.03 mM for all the tested samples. The absorbance peaks correspond to a π–π* charge transfer transition in the organic dyes. The absorption maximum (λ_{max}) of

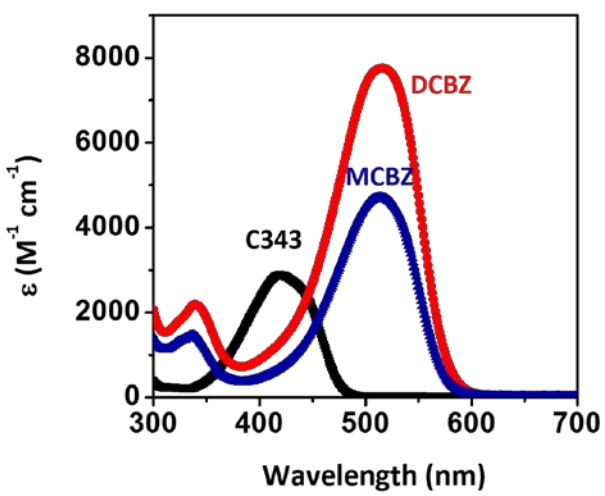

Fig. 1 Absorption spectra of C343, MCBZ, and DCBZ in ethanol. The concentration of each dye in ethanol is 0.03 mM for all the samples.

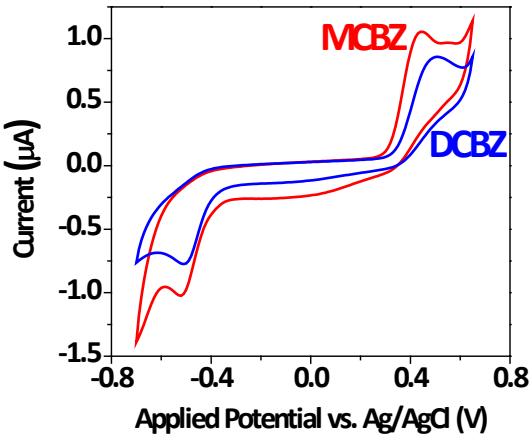

(A)

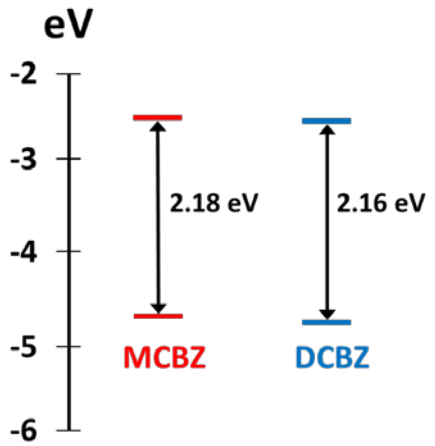

(B)

Fig. 2 (A) Cyclic voltammograms and (B) estimated band-structures of MCBZ and DCBZ.

C343 is observed at 419 nm with a molar extinction coefficient (ε_{max}) of 1.91×10^4 $M^{-1}cm^{-1}$. MCBZ absorbs a large number of photons with a longer wavelength between 400 and 600 nm (λ_{max} of MCBZ is 516 nm) and shows a high ε_{max} value of 4.23×10^4 $M^{-1}cm^{-1}$. In contrast, DCBZ exhibits an ε_{max} value of 6.77×10^4 $M^{-1}cm^{-1}$ at 516 nm without showing a peak shift compared to MCBZ.

A more detailed understanding of the energy level of the highest occupied molecular orbital (HOMO) and lowest occupied molecular orbital (LUMO) can provide essential information regarding the charge transfer kinetics. The energy level of HOMO (E_{HOMO}) can be approximated by measuring the oxidation potential (E_{OX}) of the dye by cyclic voltammetry (Fig. 2(A)). The E_{OX} of MCBZ and DCBZ is 0.39 and 0.42 V vs. NHE, respectively. These values are converted to the E_{HOMO} of MCBZ and DCBZ on an absolute scale of -4.69 and -4.72 eV, respectively, with comparing to the redox potential of ferrocene as a reference reaction. The energy level of LUMO (E_{LUMO}) is given by $E_{LUMO} = E_{HOMO} - E_g$, where Eg is the band-gap energy of each photosensitizer estimated from absorbance data. Table S1 lists the electronic absorption properties and electrochemical parameters of MCBZ and DCBZ. Their apparent band structures are presented in Fig. 2(B). As shown in their band diagrams, the band structures of MCBZ and DCBZ are not remarkably different from each other. Thus, the E_g and E_{LUMO} are not regarded as the factors to determine the differences in the photovoltaic performance of MCBZ and DCBZ.

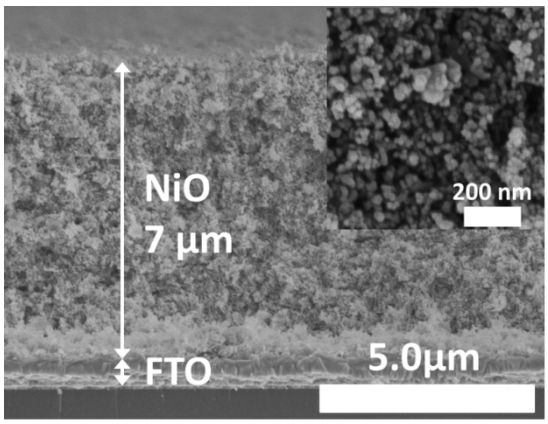

Fig. 3 Cross section SEM image of a NiO/FTO electrode prepared using the doctor blade method. The in-set shows a high resolution SEM image of NiO nanoparticles.

Adsorption on NiO films.

To fabricate the dye sensitized photocathodes, the NiO-coated FTO glass substrates are dipped in ethanol solutions of each dye. Before dyeing, the mesoporous NiO film is deposited on FTO glass substrates using the doctor blade method. S. Ito et al. introduced a novel method for preparing a transparent TiO_2 paste with α-terpineol and ethyl cellulose[9]. This method is used to prepare a NiO paste to fabricate a nanocrystalline layer for the photoactive electrodes of p-type DSSCs. The NiO photocathodes are well fabricated using the prepared NiO paste without cracking and peeling-off. Fig. 3 shows a SEM image of a cross-section of the NiO/FTO electrode. The NiO film does not contain any aggregates, and the nanoparticles are dispersed homogeneously throughout the entire layer (inset of Fig. 3). The thickness of the mesoporous NiO layer on FTO is approximately 7 μm. No cracking or peeling-off are observed on the fabricated NiO nanocrystalline layers after dipping the photocathode into the dyeing solution. Fig. 4 shows the XRD patterns of the NiO-coated FTO substrate. The characteristic peaks correspond to the rock salt-structured NiO with crystallographic preferred orientations. The XRD patterns shows only the presence of rock salt-structured NiO without other crystalline structures.

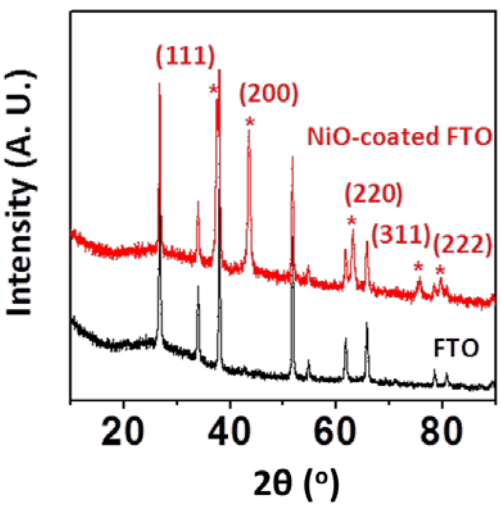

Fig. 4 XRD patterns of the FTO and NiO/FTO electrodes.

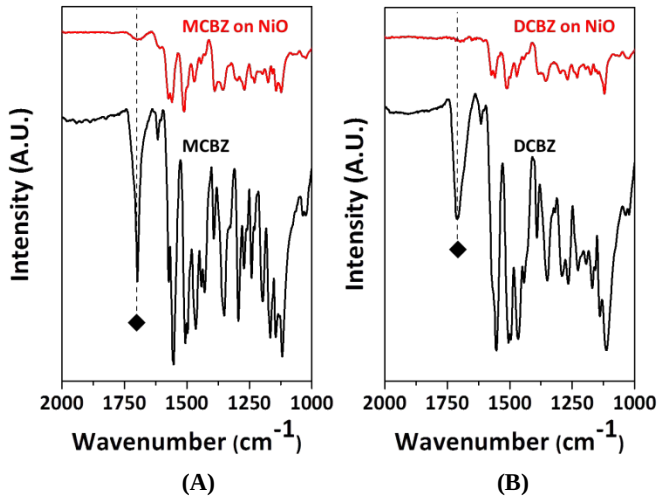

Fig. 5 FT-IR spectra of (A) MCBZ & MCBZ on NiO and (B) DCBZ & DCBZ on NiO. ◆ indicates the C=O stretching peak at 1710 cm^{-1}.

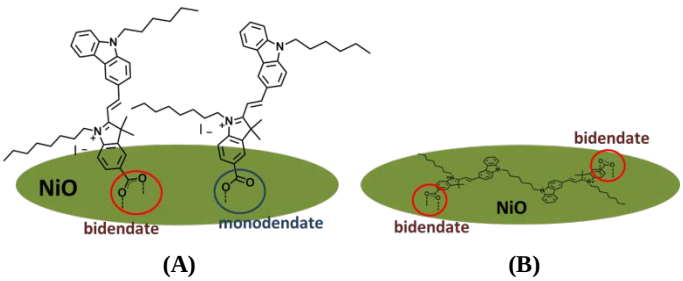

Fig. 6 Schematic diagrams of the adsorption of (A) MCBZ and (B) DCBZ on the surface of NiO.

The annealed NiO electrodes are immersed in each dye solution as the loading photosensitizer. The C343 photosensitizer adsorbs well on metal oxide with a carboxylic anchoring group in their structure (Fig. S1). The adsorption mechanism of MCBZ and DCBZ on NiO is investigated by performing FT-IR spectroscopy. Fig. 5 shows the FT-IR spectra of the photosensitizer itself and photosensitizer on NiO. FT-IR spectroscopy reveals that MCBZ and DCBZ has a C=O stretching peak at 1710 cm^{-1}, which is in the carboxylic anchoring group. As shown in Fig. 5(A), this peak is reduced significantly when MCBZ is adsorbed on NiO. This suggests that most of the MCBZ is adsorbed on NiO with a bidendate bridging structure, as shown in the left sketch in Fig. 6(A). A small amount of MCBZ is adsorbed with the monodendate mode, which yields a small peak in the FT-IR spectra at 1710 cm^{-1}. Interestingly, the peak for the C=O stretching band have decreased significantly when DCBZ is adsorbed on NiO, which means that DCBZ is adsorbed parallel to the NiO surface with a bidendate bridging structure (Fig. 6(B)). In particular, double anchoring of DCBZ leads to strong electronic coupling with NiO. This enhanced electronic coupling can cause significant enhancement of the injection of the photo-generated hole from the photosensitizer to NiO. The amounts of dye loaded on the NiO electrode films are determined by UV-Vis spectroscopy, and the results are summarized in Table 1. Each dye is detached from mesoporous NiO film using a 0.1 mM KOH solution. 1.44×10^{-4} mol/cm^3 of C343 is loaded on NiO, which is the largest value among the samples tested. The amount of MCBZ and DCBZ is 7.69×10^{-5} and 2.21×10^{-5} mol/cm^3, respectively. MCBZ with mono-anchoring moiety might be adsorbed vertically on

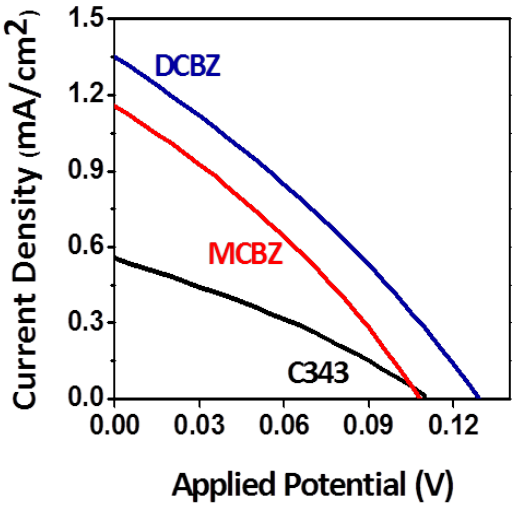

Fig. 7 Current density-voltage (J-V) characteristics of C343, MCBZ, and DCBZ sensitized solar cells under simulated solar light illumination (AM 1.5, 100 mW/cm^2).

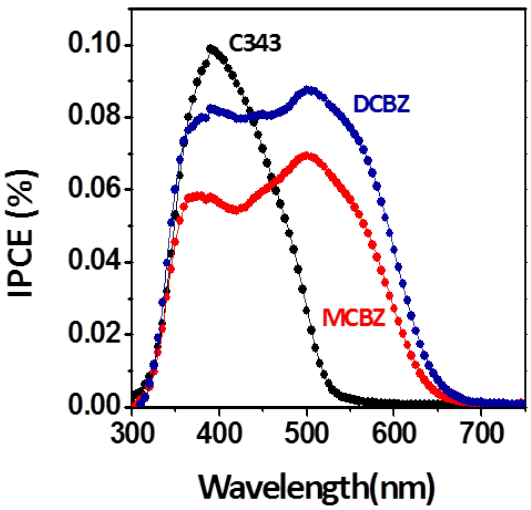

Fig. 8 IPCE curves for C343, MCBZ, and DCBZ sensitized solar cells.

the NiO surface. On the other hand, because DCBZ has two anchoring moieties at the opposite position of the chromophore, it might be adsorbed along the NiO surface. Therefore, larger amounts of MCBZ are adsorbed on the NiO electrode than DCBZ.

Photovoltaic performances of p-type DSSCs

The photocurrent density-voltage (J-V) characteristics of the C343, MCBZ and DCBZ sensitized photovoltaic cells under the illumination of AM 1.5G solar simulated light are examined (Fig. 7). Table 1 lists the short circuit current density (J_{sc}), open circuit voltage (V_{oc}), fill factor (FF), and overall efficiency of power conversion (η). C343, which is generally used as a photosensitizer for p-type DSSCs[2c, 2d], shows the lowest photovoltaic performance with J_{SC}, V_{OC} and FF values of 0.558 mA/cm^2, 0.1122 V and 0.31, respectively, to give a η value of 0.0194. These results show good agreement with the results

Table 1 Photoelectrochemical parameters for each DSSC under simulated solar light illumination (AM 1.5, 100 mW/cm^2). M is the amount of adsorbed dye on NiO.

Dye	J_{sc} (mA/cm^2)	V_{oc} (V)	FF (%)	η (%)	M (mol/cm^3)
C343	0.56 (±0.010)	0.11 (±0.001)	31.02 (±0.209)	0.0194 (±0.0003)	1.44×10^4
MCBZ	1.16 (±0.062)	0.110 (±0.006)	30.83 (±0.249)	0.0387 (±0.0007)	7.69×10^5
DCBZ	1.35 (±0.009)	0.13 (±0.002)	30.96 (±0.082)	0.0538 (±0.0007)	2.21×10^5

reported previously[2c, 2d, 5]. MCBZ provides better performance, showing double the J_{SC} value than C343, despite twice as much C343 being loaded on NiO than MCBZ. The absorbance experiments showed that MCBZ absorbs larger amounts of visible light photons than C343. These photophysical properties of MCBZ result in better photovoltaic performance than the C343-sensitized solar cells under simulated solar light irradiation. DCBZ shows better solar energy conversion efficiency than MCBZ, showing higher J_{SC} and V_{OC} values, despite the smaller amount of DCBZ loaded on NiO than MCBZ. The V_{OC} of the DCBZ-sensitized solar cell is higher than that of the MCBZ-sensitized cell. The increase in electron injection efficiency and the decrease in charge recombination probability between the redox couple and metal oxide might increase the V_{OC}[10]. Because DCBZ has two anchoring moieties at the opposite position of the chromophore, it might occupy more adsorption sites on the NiO surface over a wider region than the MCBZ dye. Bi-anchoring leads to stronger electronic coupling between DCBZ and NiO compared to that between MCBZ and NiO. This enhancement of electron coupling between DCBZ and NiO leads to the injection of photo-generated holes in DCBZ into the valence band of NiO with rapid charge transfer kinetics, leading to the generation of a high photo-current in p-type DSSCs. Moreover, the bi-anchoring structure of DCBZ helps decrease the probability of charge recombination at the interfacial region between NiO and the electrolyte. As shown in Scheme 2, there is a long - C_6H_{12} - linkage connecting the two monomers in DCBZ. This long chain enables DCBZ to cover more of the NiO surface than MCBZ, blocking charge transfer between NiO and the electrolyte. The synergistic effects of the enhanced electron injection efficiency and reduced charge recombination probability leads a DCBZ sensitized solar cell with a higher V_{OC}.

Incident photon to current efficiency (IPCE) measurements are conducted to further understand the photovoltaic cell performance of the DSSCs. Fig. 8 shows the IPCE results of the C343, MCBZ and DCBZ sensitized solar cells. The IPCE is calculated by measuring the photocurrent of each cell at different levels of monochromatic excitation. The photocurrent action spectra match the absorbance spectra of the corresponding photocathode, as shown in Fig. 1. Although C343 produces a large photo-current under the irradiation of visible light with a short wavelength (~ 400 nm), it does not adequately cover longer wavelengths (> 500 nm). This explains the poor photovoltaic performance of C343-sensitized solar cells under irradiation with simulated solar light. MCBZ and DCBZ, however, generate a photocurrent over a wide wavelength range between 300 and 700 nm, which yield better solar cells than the C343-sensitized cells. In particular, DCBZ produces a larger number of charges than MCBZ due to the synergic effect of the enhanced electron injection efficiency and reduced charge recombination probability.

The overall charge transfer resistance in the photoanode devices can be estimated by electrochemical impedance spectroscopy (EIS),

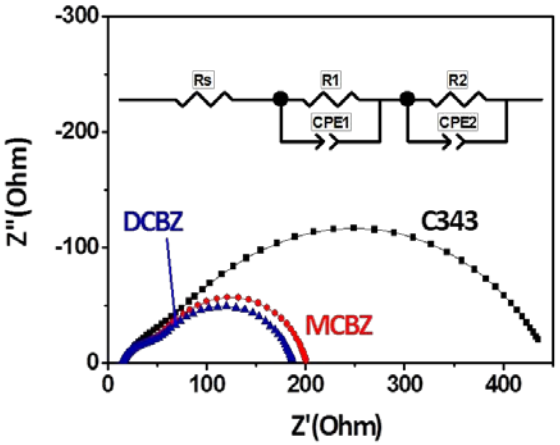

Fig. 9 Nyquist plots for C343, MCBZ, and DCBZ sensitized solar cells under the illumination of simulated solar light (AM 1.5, 100 mW/cm^2). The inset shows the equivalent circuit of the DSSCs.

Table 2 Resistance extracted from the fitted results of the EIS spectra for each p-type DSSC[a]

Dye	R_S (Ω)	R_1 (Ω)	R_2 (Ω)
C343	17.49 (±0.723)	36.65 (±0.856)	410.3 (±5.236)
MCBZ	16.31 (±0.612)	38.98 (±0.731)	145.9 (±1.963)
DCBZ	13.93 (±0.854)	35.28 (±0.845)	139.7 (±1.478)

[a]R_s: ohmic serial resistance, R_1: carge transfer resistance at the Pt anode, R_2: charge transfer resistance at the NiO/dye/electrolyte interface

which is useful for quantifying the interfacial electrochemical behaviour of DSSCs[11], QDSSCs[12], and photoelectrochemical cells[13]. Fig. 9 presents Nyquist plots of the C343-, MCBZ- and DCBZ-sensitized solar cells. The ohmic serial resistance (R_S) corresponds to the electrolyte and FTO resistance, and the resistances, R_1 and R_2, denote the charge transfer process occurring at the Pt counter electrode and NiO/dye/electrolyte interface, respectively. Table 2 lists the extracted resistances for the circuit elements. Two semicircles are observed for each Nyquist plot, which are assigned to interfacial electrochemical charge transfer on the Pt anode (at higher frequency) and photocathode (at lower frequency). Their radius is strongly related to the faradaic Red/Ox charge transfer resistance of each electrode. No significant change in the radius of the semicircle at higher frequencies is observed within the Nyquist plot for each photovoltaic cell because the Pt-coated counter electrode is used for all experiments. On the other hand, R_2 changes remarkably according to the type of photosensitizer. C343 exhibits the highest charge transfer resistance on the photocathode under solar light irradiation (R_2 of C343 is 410.3 Ω**)**. The use of MCBZ reduces the R_2 value of the DSSCs (145.9 Ω) remarkably because the optical properties of the MCBZ dye are more suitable for solar energy conversion than those of C343. Furthermore, DCBZ shows the lowest R_2 value in the impedance results because of

the synergic effect of enhanced electron injection efficiency and the reduced charge recombination probability. These findings are in agreement with the photocurrent measurement presented above.

Conclusions

This study evaluates a suitable organic dye for producing high performance p-type DSSCs. The photovoltaic properties of MCBZ and DCBZ with different numbers of anchoring groups in their chromophores are examined to determine the effects of the molecular structure of the organic dye on the solar energy conversion efficiency. MCBZ absorbs a larger number of photons with a longer wavelength between 400 and 600 nm. The absorption properties of MCBZ allow the production of much better p-type DSSCs than conventional C343-sensitized solar cells. Furthermore, DCBZ exhibits better photovoltaic performance, showing higher J_{SC}, V_{OC} and η values, and lower charge transfer resistance over the photoanode than the mono-anchored MCBZ dye sensitized solar cells.

Acknowledgements

This study was supported by the "New & Renewable Energy Core Technology Program" of the Korea Institute of Energy Technology Evaluation and Planning (KETEP) granted financial resource from the Ministry of Trade, Industry & Energy (No. 20133010011750) and Basic Science Research Program through the National Research Foundation of Korea (NRF) funded by the Ministry of Education, Science and Technology, Republic of Korea (grant number: NRF-2012R1A2A2A01014395).

Notes and references

[a]Department of Chemical Engineering, Yeungnam University, Gyeongsangbuk-do, South Korea 712-749

Jae Hong Kim Tel: +82-53-810-2521 E-mail: jaehkim@ynu.ac.kr

Hyeong Jin Yun Tel: +82-53-810-3716 E-mail: hjyun@ynu.ac.kr

† Electronic Supplementary Information (ESI) available: Molecular structure of C343 (Fig. S1), mass spectra of MCBZ and DCBZ, and electrochemical parameters of MCBZ and DCBZ. See DOI: 10.1039/b000000x/

References and Notes

1. (a) B. O'Regan and M. Grätzel, *Nature*, 1991, **353**, 737; (b) M. Grätzel, *Nature*, 2001, **414**, 338.
2. (a) J. J. He, H. Lindstrom, A. Hagfeldt and S. E. Lindquist, *J. Phys. Chem. B*, 1999, **103**, 8940; (b) P. Qin, H. Zhu, T. Edvinsson, G. Boschloo, A. Hagfeldt and L. Sun, *J. Am. Chem. Soc.*, 2008, **130**, 8570; (c) F. Odobel, L. Le Pleux, Y. Pellegrin and E. Blart, *Acc. Chem. Res.*, 2010, **43**, 1063; (d) F. Odobel, Y. Pellegrin, E. A. Gibson, A. Hagfeldt, A. L. Smeigh and L. Hammarström, *Coord. Chem. Rev.*, 2012, **256**, 2414; (e) Z. Ji, G. Natu, Z. Huang, O. Kokhan, X. Zhang and Y. Wu, *J. Phys. Chem. C*, 2012, **116**, 16854; (f) H. Tian, J. Oscarsson, E. Gabrielsson, S. K. Eriksson, R. Lindblad, B. Xu, Y. Hao, G. Boschloo, E. M. J. Johansson, J. M. Gardner, A. Hagfeldt, H. Rensmo and L. Sun, *Sci. Rep.*, 2014, **4**, 4282.
3. (a) J. J. He, H. Lindstrom, A. Hagfeldt and S. E. Lindquist, *Sol. Energy Mater. Sol. Cells*, 2000, **62**, 265; (b) A. Nattestad, A. J. Mozer, M. K. R. Fischer, Y. B. Cheng, A. Mishra, P. Baeuerle and U. Bach, *Nat. Mater.*, 2010, **9**, 31.
4. L. Li, L. L. Duan, F. Y. Wen, C. Li, M. Wang, A. Hagfeld and L. C. Sun, *Chem. Commun.*, 2012, **48**, 988.
5. (a) M. Yu, T. I. Draskovic and Y. Wu, *Phys. Chem. Chem. Phys.*, 2014, **16**, 5026; (b) J. Warnan, Y. Pellegrin, E. Blart, L. Zhang, A. Brown, L. Hammarström, D. Jacquemin and F. Odobel, *Dyes Pigment.*, 2014, **105**, 174; (c) D. Xiong, Z. Xu, X. Zeng, W. Zhang, W. Chen, X. Xu, M. Wang and Y.-B. Cheng, *J. Mater. Chem.*, 2012, **22**, 24760.
6. (a) M. S. Kim, H. S. Yang, D. Y. Jung, Y. S. Han and J. H. Kim, *Colloids Surf. A. Physicochem. Eng. Aspects*, 2013, **420**, 22; (b) A. Michaleviciute, M. Degbia, A. Tomkeviciene, B. Schmaltz, E. Gurskyte, J. V. Grazulevicius, J. Boucle and F. Tran-Van, *J. Power Sources*, 2014, **253**, 230; (c) A. Venkateswararao, K. R. J. Thomas, C.-P. Lee, C.-T. Li and K.-C. Ho, *ACS Appl. Mater. Interfaces*, 2014, **6**, 2524.
7. (a) M. Cheng, X. Yang, C. Chen, J. Zhao, Q. Tan and L. Sun, *Phys. Chem. Chem. Phys.*, 2013, **15**, 17452; (b) C. J. Wood, M. Cheng, C. A. Clark, R. Horvath, I. P. Clark, M. L. Hamilton, M. Towrie, M. W. George, L. Sun, X. Yang and E. A. Gibson, *J. Phys. Chem. C*, 2014, **118**, 16536.
8. S. S. Park, Y. S. Won, Y. C. Choi and J. H. Kim, *Energy Fuels*, 2009, **23**, 3732.
9. S. Ito, P. Chen, P. Comte, M. K. Nazeeruddin, P. Liska, P. Péchy and M. Grätzel, *Prog. Photovoltaics*, 2007, **15**, 603.
10. Z. Ning, Y. Fu and H. Tian, *Energy Environ. Sci.*, 2010, **3**, 1170.
11. (a) J. Halme, P. Vahermaa, K. Miettunen and P. Lund, *Adv. Mater.*, 2010, **22**, E210; (b) F. Fabregat-Santiago, J. Bisquert, E. Palomares, L. Otero, D. Kuang, S. M. Zakeeruddin and M. Grätzel, *J. Phys. Chem. C*, 2007, **111**, 6550.
12. (a) V. González-Pedro, X. Xu, I. Mora-Seró and J. Bisquert, *ACS Nano*, 2010, **4**, 5783; (b) H. J. Yun, T. Paik, M. E. Edley, J. B. Baxter and C. B. Murray, *ACS Appl. Mater. Interfaces*, 2014, **6**, 3721.
13. H. J. Yun, H. Lee, J. B. Joo, W. Kim and J. Yi, *J. Phys. Chem. C*, 2009, **113**, 3050.